

# Radiationless Travelling Waves In Saturable Nonlinear Schrödinger Lattices

T.R.O. Melvin<sup>1</sup>, A.R. Champneys<sup>1</sup>, P.G. Kevrekidis<sup>2</sup> and J. Cuevas<sup>3</sup>

<sup>1</sup> *Department of Engineering Mathematics, University of Bristol, BS8 1TR, UK*

<sup>2</sup> *Department of Mathematics and Statistics, University of Massachusetts, Amherst, MA 01003-4515, USA*

<sup>3</sup> *Grupo de Física No Lineal, Departamento de Física Aplicada I, Escuela Universitaria Politécnica, Virgen de África, 7, 41011 Sevilla, Spain*

The longstanding problem of moving discrete breathers (intrinsic localised modes) in nonlinear Schrödinger lattices is revisited. The context is photorefractive crystal lattices with saturable nonlinearity whose generalised Peierls-Nabarro barrier vanishes for isolated coupling strength values. *Genuinely localised travelling waves* (i.e., moving discrete breathers) are computed as a function of the system parameters *for the first time*. The relevant solutions exist only for finite velocities.

PACS numbers:

Recently, the topic of discrete solitons (intrinsic localised modes) in photorefractive materials has received significant attention, see [1] for a review. This interest was initialized by the experimental realization of two-dimensional photonic periodic crystal lattices [2] in which solitons were observed [3, 4]. Further work has revealed a wealth of additional coherent structures such as dipoles, quadrupoles, soliton trains, vector, necklace and ring solitons, see e.g. [5, 6, 7, 8]. Since photorefractive materials feature so-called saturable nonlinearity, these results for periodic lattices have spawned a parallel interest in genuinely *discrete* saturable nonlinear lattices [9, 10, 11]. One particularly intriguing result of these studies is that the stability properties of the localized modes are substantially different to their regular discrete nonlinear Schrödinger (DNLS) analogs. In DNLS it is well-known [12, 13, 14] that site-centered localised modes are always stable, while intersite-centered modes are unstable (and are only stabilized in the continuum limit where these two branches degenerate into the well-known continuum sech-soliton of the integrable cubic NLS). For the photorefractive nonlinearity, depending on the coupling strength, the inter-site centered modes may have lower energy than their onsite counterparts. Hence, one should expect that the ensuing sign reversal of the so-called Peierls-Nabarro (PN) energy barrier  $\Delta E = E_{IS} - E_{OS}$  (where the subscripts denote intersite and onsite respectively) should cause an exchange between the linear stability properties of the two modes.

A related, even more fundamental, question in nonlinear lattice models of DNLS type is whether exponentially localized self-supporting excitations that move with a constant wave speed can exist, so called *moving discrete breathers*. For continuum models this question is in some sense trivial since the equations posed in a moving frame remain of the same fundamental type. Yet for lattices, passing to a moving frame leads to so-called advance-delay equations that are notoriously hard to analyse. One recent (negative) result in this direction [15] for the so-called Salerno model, shows that, starting from the integrable Ablowitz-Ladik equation,

mobile discrete breathers acquire non-vanishing tails as soon as parameters deviate from the integrable limit. Hence exponentially localised fundamental (single humped) moving discrete breathers cannot be constructed. While these results settle a long-standing controversy, see e.g. [16, 17, 18], they are also somewhat unsatisfactory since they do not give conditions under which moving discrete breathers might exist for generic, non-integrable lattices.

In the arguably simpler problem of kinks in Frenkel-Kontrova lattices (also known as discrete Klein-Gordon models), genuinely travelling fundamental ('charge one') topological solitons are known *not* to occur unless there is a "competing" nonlinearity that causes vanishings of the PN barrier; see e.g. [19, 20]. Drawing an analogy from this, for DNLS models with pure cubic nonlinearity, the PN barrier never disappears, so one should not expect genuinely localised moving solitons (in some sense anticipating the above-mentioned negative result). However the present saturable model has a nonlinear term in its denominator, which, under Taylor expansion, is effectively cubic for low intensities but exhibits saturation for large intensities. This effective competition between nonlinear terms leads to the possibility of the vanishing of the PN barrier, and hence suggests this model as a good candidate for finding moving discrete breathers. Such a search is the theme of this Letter.

We start by examining the existence of stationary localized modes as the strength of inter-site coupling is varied, initializing our computations from the anti-continuum limit, where explicit solutions are available. A linear stability analysis of the solutions is carried out, and we find that the regime of stability-instability alternation does not coincide with the vanishings of the PN barrier but rather with the vanishings of the grand-canonical free-energy of the system  $G = E - \Lambda P$ , where  $\Lambda$  is the frequency (chemical potential) of the solution and  $P$  is its  $l^2$  norm. After identifying this sequence of *transparent points*, we proceed to obtain, for the first time in discrete nonlinear Schrödinger type models, genuinely localized, single-humped, uniformly traveling solutions in

their vicinity. This is done by examining travelling solutions as embedded solitons [21], such that while resonant with the linear spectrum in the travelling frame, the tail amplitude can vanish for isolated, definitely non-zero values of the speed, for a given set of system parameters. This is reminiscent of recent work in the Klein-Gordon context [22], where the so-called Stokes constant is shown to vanish for isolated values of the speed, indicating the presence of travelling localised solutions.

The model of interest, as discussed above will be a discrete lattice with photorefractive nonlinearity, namely,

$$i\dot{u}_n = -\varepsilon\Delta_2 u_n + \frac{\beta}{1 + |u_n|^2} u_n. \quad (1)$$

Here,  $\varepsilon$  denotes the coupling strength between adjacent sites and  $\beta$  is the coefficient of the nonlinearity (proportional to the voltage in photorefractive crystals) and can be scaled out for our purposes. We will therefore set  $\beta = 1$  in what follows. We seek stationary solutions of the form  $u_n = e^{-i\Lambda t} v_n$ , starting from the so-called anti-continuum (AC) limit  $\varepsilon = 0$ . In that limit the principal solutions of interest are the onsite solution with  $u_{n_0} = \pm\sqrt{(1/\Lambda) - 1}$ , (all other sites bearing vanishing amplitudes) and the intersite-centered solution with  $u_{n_0} = u_{n_0+1} = \pm\sqrt{(1/\Lambda) - 1}$  and zero amplitudes elsewhere. We initialize these exact profiles from the AC limit and subsequently use continuation in  $\varepsilon$  to solve the stationary equations for the solution profile via Newton's method for finite  $\varepsilon$ . We also examine the linear stability of the obtained modes using linearization around a solution profile  $v_n^0$  of the form:  $u_n = e^{-i\Lambda t} [v_n^0 + \delta(a_n e^{\lambda t} + b_n e^{\lambda^* t})]$ , and resolving the ensuing matrix eigenvalue problem ensuing to  $O(\delta)$  for the eigenvalue  $\lambda$  and the eigenvector pair  $(a_n, b_n^*)$  (where  $*$  stands for complex conjugation). In what follows, we will also use the (Hamiltonian) energy of solutions,

$$E = \sum_n [\varepsilon |u_{n+1} - u_n|^2 + \log(1 + |u_n|^2)], \quad (2)$$

and the  $l^2$ -norm,  $P = \sum_n |u_n|^2$ .

Our stationary calculations as a function of the intersite coupling (rather than of the frequency as in [9]) are shown in Fig. 1. The left panels of the figure show the key imaginary eigenvalues of the problem, while the bottom right panel shows the maximal real eigenvalues (the top right graph will be explained shortly). A solid line is used in the figures to represent the inter-site centered (IS) mode, and a dashed line the onsite-centered (OS) mode. Observe that for small values of  $\varepsilon$  the OS mode is stable while the intersite mode is unstable. Consider the OS mode. At  $\varepsilon \approx 0.1$ , an eigenvalue emerges from the band edge of the continuous spectrum at  $\lambda = i\Lambda$ , and approaches the origin of the spectral plane. This feature also occurs in the pure cubic DNLS but the eigenvalue only arrives at the origin of the spectral plane as  $\varepsilon \rightarrow \infty$

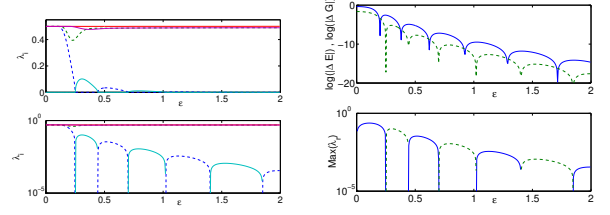


FIG. 1: (Color Online) The left panels show the key imaginary eigenvalues for the onsite (dashed line) and the intersite (solid line) mode as a function of  $\varepsilon$  (top, on a linear scale, bottom on an exponential scale). The band edge of the continuous spectrum is at  $\Lambda = 0.5$ . From there bifurcates an eigenmode for  $\varepsilon > 0.1$  (for the onsite case) which arrives at the origin of the spectral plane for  $\varepsilon = 0.25$  (and becomes real). On the contrary for the intersite solution a (previously real) eigenmode exits as imaginary for  $\varepsilon > 0.25$ . These modes alternate again for  $\varepsilon = 0.445$ ,  $\varepsilon = 0.7$  etc. The real parts of the corresponding eigenvalues are shown in the bottom right panel. The top right panel shows  $\log(|\Delta E|)$  between onsite and intersite modes, and by dashed line the quantity  $\log(|\Delta G|)$ , where  $G = E - \Lambda P$  (see text for details).

(the continuum limit). Here the eigenvalue arrives at the origin for  $\varepsilon \approx 0.25$ , becomes real for  $0.25 < \varepsilon < 0.445$ , then becomes imaginary again for  $0.445 < \varepsilon < 0.7$ , then real again, etc. Furthermore, this alternation of stability occurs hand-in-hand with the alternation of stability of the IS mode, which starts out unstable, becomes stable, then unstable again, with the transitions occurring at precisely the same  $\varepsilon$ -values. Note from the figure that stability alternation occurs, *not* at the points of vanishing of the PN energy barrier; but when the *grand-canonical energy barrier* of the model  $\Delta G$  between the IS and OS modes vanishes. This provides an alternative viewpoint to the results of [9]. At these very points, the relevant eigenvalue (pertaining to translation) crosses zero, instantaneously restoring an effective translational invariance in the model. Thus these are *transparent points* where there is a one-dimensional family of localised solutions, obtained from each other by translation, of which the OS and IS modes are just two examples.

Intuitively, one might expect that the transparent points represent parameter values at which genuinely travelling localised solutions of the photorefractive lattice might bifurcate with zero wave speed. Hence we shall look for solutions to Eq. (1) near such points using a travelling wave substitution  $u_n(t) = \psi(n - ct)e^{i(kn - \Lambda t)}$ . This leads to the advance-delay equation in the travelling co-ordinate  $z = n - ct$

$$-ic\psi'(z) = (2\varepsilon - \Lambda)\psi(z) - \varepsilon(\psi(z+1)e^{ik} + \psi(z-1)e^{-ik}) + \frac{1}{1 + |\psi(z)|^2}\psi(z), \quad (3)$$

where  $'$  denotes differentiation with respect to  $z$ . Equa-

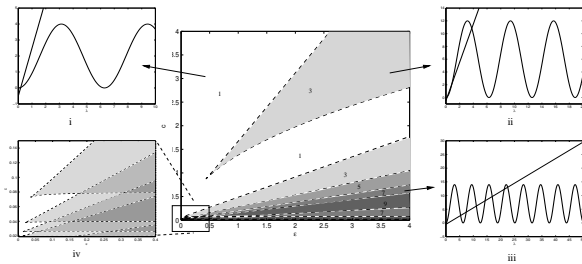


FIG. 2: Intersections of the single and double root conditions (see text) for  $\Lambda = 0.5$  and varying  $c$  and  $\varepsilon$ . The shaded area shows where there is more than one branch of linear waves. Values indicate the number of roots of (4). Subplots show left and right hand sides of (4) for  $(\varepsilon, c) = (1, 3)$ , one root (i),  $(3, 3)$ , three roots (ii) and  $(3.5, 0.6)$ , seven roots (iii). (iv) displays the overlapping of the bands for small  $\varepsilon$  and  $c$ , only the first six bands have been shown.

tion (3) is rotationally invariant, therefore the transformation  $\psi(z) = \tilde{\psi}(z)e^{-ikz}$  can be used to obtain the same equation as above for  $\tilde{\psi}$  and  $\tilde{\Lambda} = kc + \Lambda$ . Therefore,  $k = 0$  will be used hereafter in (3) without loss of generality. The linear spectrum is obtained by substitution of  $\psi(z) = e^{i\lambda z}$  into the linear part of Eq. (3))

$$c\lambda + \Lambda - 1 = 4\varepsilon \sin^2\left(\frac{\lambda}{2}\right) \quad (4)$$

It is interesting to note that the asymptotic behaviour of the two sides of Eq. (4) for small  $\lambda$  is such that a resonance with the linear spectral bands is unavoidable. However, in the hope of obtaining a localized solution such resonances need to be minimized and hence we need to investigate parameter regions where Eq. (4) has only one root,  $\lambda > 0$ . This can be efficiently done [20] by considering the conditions for double roots, namely  $c = 2\varepsilon \sin(\lambda)$ , which allow us to distinguish among regions with different root multiplicity. The results are plotted in Fig. 2, from which it can be seen that for each  $\varepsilon > 0$ , the number of spectral bands increases to infinity as  $c \rightarrow 0$ . This result serves to counter the naive expectation that near the transparency points, travelling solutions of small speed may exist.

The best hope for finding genuinely localised solutions is then within parameter regions of Fig. 2 in which there is a single resonance with linear waves. Such solutions would represent embedded soliton structures [20, 21] for which the radiation mode component exactly vanishes in the tail of the solitary wave. At best this could happen in a codimension-one set in parameter space, that is along discrete curves lying within the single resonance bands of Fig. 2. Solutions of this type are sought using a pseudo-spectral method, see [17, 19]. To this end, we set

$$\psi(z) = \sum_{j=1}^N a_j \cos(\omega_j z) + ib_j \sin(\omega_j z) \quad (5)$$

with  $\omega_j = \frac{2\pi j}{L}$ , to transform (3) into a system of algebraic equations in the long finite interval  $[-L/2, L/2]$ .  $a_j, b_j \in \mathbb{R}$  are the coefficient of the Fourier series, for which the ensuing algebraic equations are solved at the collocation points  $z_m = \frac{Lm}{2(N+1)}$ . The solution is obtained by means of the Powell hybrid method [23], with an error tolerance of  $10^{-13}$ . From the resulting  $a_j, b_j$ 's,  $\psi(z)$  can be reconstructed and numerically continued using AUTO [24] with an error tolerance of  $10^{-10}$  to investigate the effect of varying parameters on the solution shape and its tail amplitude. Generally, the thus obtained solutions will be weakly nonlocal ones with non-zero oscillatory tails. However, appending an additional tail condition for the solution, yielding a signed measure  $\Delta$  of the amplitude of the tail, we can obtain truly localised solutions as isolated zeros of this function  $\Delta$ . Given our choice of phase in the substitution (5) that the real component of  $\psi$  is odd about  $z = L/2$  (and vice versa for the imaginary component), a good choice for such a tail amplitude measure is  $\Delta = \text{Im}(\psi(\frac{L}{2}))$ .

Continuation of quasi-breather solutions as  $\varepsilon$  varies is shown as a function of  $1/\varepsilon$  in Fig. 3 (top left). Note the topological distinction between branches the ‘S’-shaped branches that contain true zeros of  $\Delta$  and the ‘U’ or ‘n’-shaped branches that do not [25]. Once the isolated points where the tail disappears are found, these can be continued in any pair of desired parameters, e.g.  $(\varepsilon, c)$  by appending the condition  $\Delta = 0$  to the numerical problem. Thus, we can construct the parametric diagram of the existence of such *genuinely travelling* (with constant prescribed speed), yet *truly localized* (i.e., radiationless due to  $\Delta = 0$ ) solutions. A regular sequence of branches so-obtained are found as  $\varepsilon$  increases, the first three of which are shown in the top right panel of Fig. 3. Notice that each branch terminates (as it should) at the edges of the multi-spectral bands. Nevertheless, at the low- $c$  end the branches are close to straight lines which if continued to zero wave speed would hit the transparent points. Thus, while there is no actual bifurcation as such of travelling breathers from these transparent points, their presence has a strong influence.

The lower four panels of Fig. 3 show solution profiles on the first (lowest  $\varepsilon$ ) branch of localised solutions. Note from the upper row how the profile delocalizes when the edge of the multi-resonance band is reached. Any attempt to continue zero-tail solutions into the band resulted in lack of convergence for large enough  $L$  and  $N$ . Figure 4 shows the result of direct integration of a representative solution on each of the relevant branches, clearly illustrating their genuinely travelling nature, and indicating that they are stable against the perturbation introduced by numerical discretization.

In conclusion, to our knowledge, this is the *first time* genuinely localised travelling waves (so-called *moving discrete breathers*) have been found in a discrete lattice of nonlinear Schrödinger type. While it is true that our con-

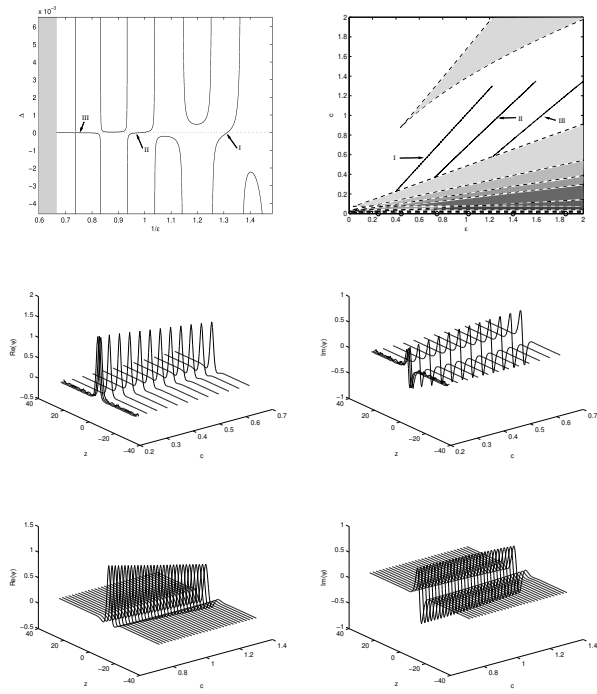


FIG. 3: (Top left) Continuation of quasi breathers for various values of  $1/\varepsilon$  showing three zeros in  $\Delta$  for  $c = 0.7$ ,  $\Lambda = 0.5$ ,  $L = 60$ . Zeros of  $\Delta$  at  $\varepsilon \approx 0.76, 1.02, 1.36$ . (Top right). Continuation of the 3 zeros of  $\Delta$ , varying  $\varepsilon$  and  $c$  with  $\Lambda = 0.5$ . Circles on the  $c = 0$  axis indicate the transparency points. Middle and bottom panels show the continuation of the (real and imaginary parts of the) solution of branch I for lower and higher, respectively, values of the speed.

struction has relied on numerical continuation, we have demonstrated the robustness of the solutions we have obtained, and have provided a new rationale as to why they should exist. This rationale is based on the existence of transparent points for stationary localised modes when a generalised Peierls-Nabarro barrier vanishes. However, we have also shown that this is not enough, one also needs the wave speed to be sufficiently large to overcome the multi-spectral bands. Within each band, exponentially localised solutions occur as embedded solitons which correspond to *regular zeros* of an appropriately defined measure of the tail amplitude.

We anticipate that the principal features of the model problem studied (competing nonlinear terms for the existence of transparent points and sufficiently high wave speeds to overcome the multi-spectral bands) should be generic features a variety of similar Hamiltonian lattices. In particular, more realistic models of photorefractive crystals should be expected to behave similarly, giving the possibility of experimental observation of the waves we have constructed in photonic crystal fibres. There, the robust, radiationless nature of the new moving pulses could find significant application to future

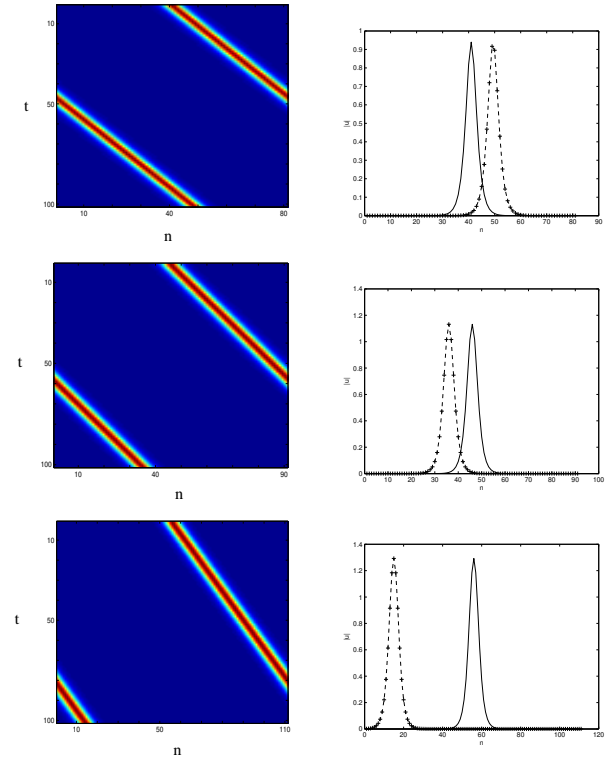


FIG. 4: (Color Online) Three examples of direct integration of the solution of branch I with  $\varepsilon = 0.911396$ ,  $c = 0.894153$  (top panels), branch II with  $\varepsilon = 1.11714$ ,  $c = 0.81$  (middle panels) and branch III with  $\varepsilon = 1.34529$ ,  $c = 0.7$  (bottom panels). The space time contour plot of the solution modulus (left panels), and the modulus before (solid) and after (dashed) the solution has moved by 100 nodes (right panels) are shown.

optical processing devices. An equally interesting theoretical question is the extension of the present ideas to two-dimensional settings [26], where deciding which directions of wave propagation within the lattice can lead to radiationless pulses will also be of interest.

- 
- [1] J.W. Fleischer, Opt. Express **13**, 1780 (2005).
  - [2] N.K. Efremidis *et al.*, Phys. Rev. E **66** (2002) 046602.
  - [3] J.W. Fleischer *et al.*, Phys. Rev. Lett. **90** (2003) 023902.
  - [4] H. Martin *et al.*, Phys. Rev. Lett. **92** (2004) 123902.
  - [5] J. Yang *et al.*, Phys. Rev. Lett. **94**, 113902 (2005).
  - [6] X. Wang, Z. Chen and P.G. Kevrekidis, Phys. Rev. Lett. **96**, 083904 (2006).
  - [7] D.N. Neshev *et al.*, Phys. Rev. Lett. **92** (2004) 123903.
  - [8] J.W. Fleischer *et al.*, Phys. Rev. Lett. **92** (2004) 123904.
  - [9] L. Hadziewski *et al.*, Phys. Rev. Lett. **90**, 033901 (2004).
  - [10] M. Stepic *et al.*, Phys. Rev. E **69**, 066618 (2004).
  - [11] J. Cuevas and J.C. Eilbeck, nlin.PS/0501050.
  - [12] P.G. Kevrekidis, K.Ø. Rasmussen and A.R. Bishop, Int. J. Mod. Phys. B **15**, 2833 (2001);
  - [13] D. N. Christodoulides, F. Lederer, and Y. Silberberg,

- Nature **424**, 817 (2003);
- [14] T. Kapitula and P. Kevrekidis, Nonlinearity **14**, 533 (2001).
  - [15] J. Gómez-Gardeñes, L.M. Floría, M. Peyrard and A.R. Bishop, Chaos **14**, 1130 (2004).
  - [16] M. Remoissenet and M. Peyrard (eds.) *Nonlinear Coherent Structures in Physics and Biology* Springer-Verlag Berlin, (1991);
  - [17] D.B. Duncan *et al.*, Physica D **68**, 1 (1993);
  - [18] M.J. Ablowitz, Z.H. Musslimani and G. Biondin, Phys. Rev. E **65**, 026602 (2002).
  - [19] A.V. Savin, Y. Zolotaryuk and J.C. Eilbeck, Phys. D. **138**, 267 (2000).
  - [20] A Aigner, A.R. Champneys and V.M. Rothos Phys. D **186**, 148 (2003).
  - [21] J. Yang, B.A. Malomed and D.J. Kaup, Phys. Rev. Lett. **83**, 1958 (1999).
  - [22] O.F. Oxtoby, D.E. Pelinovsky and I.V. Barashenkov, Nonlinearity **19**, 217 (2006).
  - [23] M.J.D. Powell. *Numerical Methods for Nonlinear Algebraic Equations*. (Gordon and Breach, 1970).
  - [24] E.J. Doedel *et al.*, AUTO97 continuation and bifurcation software for ordinary differential equations, available via: <ftp://ftp.es.concordia.ca/directory/doedel/auto>
  - [25] A.R. Champneys, J.-M. Vanden-Broeck and G.J. Lord, *J. Fluid Mech*, **454**, 403 (2002).
  - [26] R. Vicencio, M. Johansson, nlin.PS/0511003.

